Tunneling dynamics and spatial correlations of long chain growth in solid-state photochlorination of ethylene at low temperatures

E. Ya. Misochko[a]*, *C. A. Wight*[b], *E. V. Vetoshkin*[a], *and V. A. Benderskii*[a]

[a]*Institute of Chemical Physics Russian Academy of Sciences, Chernogolovka, 142432 Moscow Region, Russian Federation. Fax: +7 (095) 938 21156*

[b]*Department of Chemistry, University of Utah, Salt Lake City, Utah 84112 USA. Fax: +1 (801) 581 8433*

A novel method is described for preparing reactive cryocrystals by deposition of argon-diluted reactant beams and subsequent crystallization during evaporation of the inert gas. Photochlorination of equimolecular ethylene—chlorine mixtures obtained by this method and studied by means of kinetic UV-and IR-spectroscopy reveals activationless chain growth with mean length 300 units in the temperature range 17—45 K. Mean chain lengths greater than 100 are observed up to the conversion degree of 0.6—0.7. Comparison of the experimental data with computer simulations shows that the tunneling reaction is due to the formation of a closely packed reaction complex with high amplitudes of zero-point vibrations which lower the reaction barrier. The commensurability of reactant and product crystal lattices results in linear propagation of chains without accumulation of deformation strain. The chain termination mechanism associated with the spatial correlations of chains is discussed.

Key words: cryochemistry, solid-state reactions, photochlorination, chlorine, ethylene.

Recent progress in theoretical investigations of nuclear tunneling and its significance for low-temperature chemistry has stimulated interest in exploring different types of chemical conversions at cryogenic temperatures. The most obvious demonstration of tunneling in chemical kinetics is the predicted[1] transition of the rate constant from Arrhenius dependence to the low-temperature limit where reactant activation at the expense of thermal excitation is absent. Now there are many examples of low-temperature chemical reactions whose rate constants are independent of temperature below 50—100 K (see, e.g., reviews[2,3]). Most of them are hydrogen transfer reactions, although the model of multidimensional dynamical nuclear tunneling[4,5] predicts that the transfer of heavier particles is possible. More complex reactions may thereby proceed with measurable rate constants at $T = 0$. However, the number of such reactions is relatively small, and their mechanism needs further elucidation. According to the available experimental data, several conditions must be satisfied[6] to enable solid-state tunneling reactions of heavy particles:

1. reaction exoergicity;
2. location of reactants in neighboring lattice sites, which allows for conversion without translational diffusion;
3. existence of high-amplitude low-frequency modes that provide quantum displacement along the reaction coordinate.

Another interesting aspect of these reactions relates to the appearance of spatial correlations caused by the accumulation of products with a crystal lattice incommensurate with that of the reactants. This is manifested most distinctly for chain reactions, in which successive chain growth acts occur in neighboring lattice sites, so that they cannot be treated as independent steps. The structural relaxation is slowed down at low temperatures, so spatial correlations lead to specific features of conversion kinetics, in particular to the critical and auto-wave phenomena discussed earlier.[7—11]

Studies of several chain chemical reactions in glassy mixtures carried out in different laboratories have revealed that at temperatures below the glass transition temperature T_g chain growth is limited to 3—10 links[12—14] due to the absence of long-range ordering in reactant orientation. Long chain growth would likely occur in crystal systems if the reactants were to form an initially ordered structure[15] with packing suitable for the reaction. In particular long chain growth may be possible in mixed crystals with alternating reactant arrangement, e.g. in Hassel crystals[16]. These crystals exist for 1:1 olefin—halogen complexes. The model binary ethylene—chlorine crystal, whose structure has been calculated earlier,[17] is quasi-two-dimensional and consists of planes in which C_2H_4 and Cl_2 molecules are organized into alternating chains having a shortened distance along the shortest diagonal in the *ac*-plane (Fig. 1). A molecular reaction in

Translated from *Izvestiya Akademii Nauk. Seriya Khimicheskaya,* No. 4, pp. 687—700, April, 1993.

1066-5285/93/4204-0648 $12.50

a C_2H_4:Cl_2 complex occurs[18,19] at temperatures above 85 K in the absence of photoinitiation. This reaction results in *gauche*-1,2-dichloroethane formation with the rate constant equal to 10^{-5} s^{-1} at 90 K. The rate constant is temperature-dependent in the temperature range 90—100 K, with the activation energy of 5.7 kcal/mole.

Below 80 K the reaction only takes place upon photoinitiation and affords exclusively the *trans*-conformer,[20] which means the conversion propagation along the chain of alternating reactants is accoriding to a radical mechanism. The product is formed by the addition of the chlorine atoms belonging to the two Cl_2 molecules adjacent to C_2H_4 as a result of two consecutive exothermal reactions:

$$\begin{aligned} Cl + C_2H_4 &\longrightarrow C_2H_4Cl, \\ C_2H_4Cl + Cl_2 &\longrightarrow C_2H_4Cl_2 + Cl, \end{aligned} \qquad (1)$$

where the second stage is rate-limiting with an activation energy of 1 kcal/mole in the gas phase.[21]

The dimensions of the dichloroethane unit cell are close to those of the reactant unit cell, so that the reaction product appears in the initial lattice site and does not displace significantly neighboring molecules.[17] On the one hand, this favors linear chain propagation along the small diagonal of the *ac*-plane (Fig. 1) and, on the other hand, the formation of the product spatial chain does not seriously hinder neighboring chain growth along the same direction. The binary mixed crystals studied in refs. 17—20 provide promising objects for investigating not only low-temperature tunneling reactions, but also spatial correlations, since long-chain growth occurs up to high conversion degrees in these crystals. This prompted us to continue the research[17—20] using a new method of crystal preparation, in which the chain length and the conversion degree are much higher than in crystals obtained with the usual techniques.

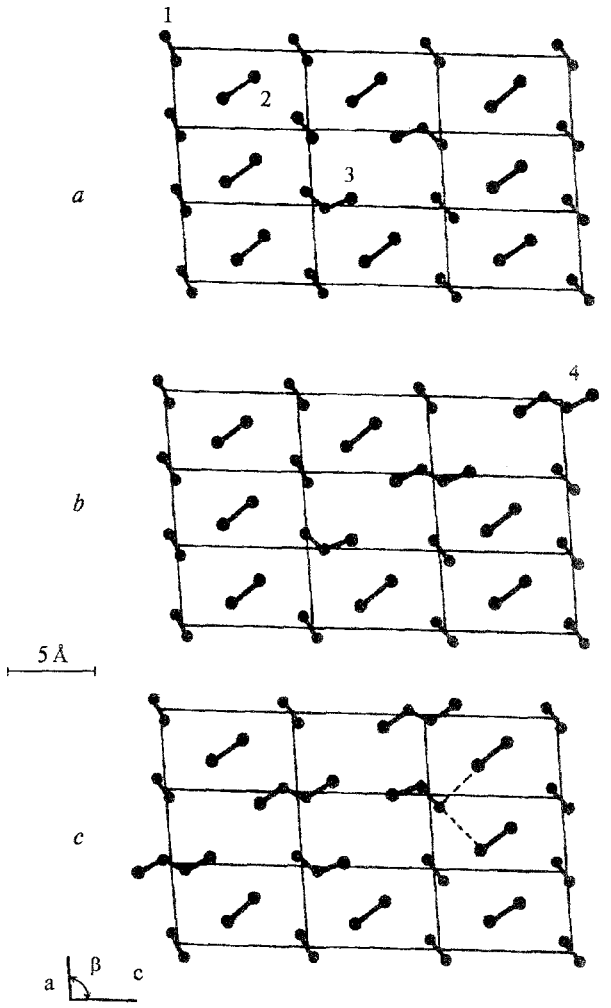

Fig. 1. Molecular arrangement in the *ac*-plane of a mixed ethylene-chlorine crystal illustrating radical pair formation (*a*), single chain growth (*b*), and chain growth in the vicinity of a product line (*c*). Molecules 1—4 are ethylene, chlorine, C_2H_4Cl radical, and *trans*-1,2-dichloroethane, respectively.

Experimental

The samples were prepared by a conventional procedure accepted in cryochemistry, viz., by simultaneous deposition of separate gas phase reactant beams (or their mixtures with argon) onto a cold substrate kept at 10^{-6} Torr vacuum. The KBr (or BaF_2) substrate was mounted with indium gaskets on a copper retainer at the cold tip of a helium cryostat equipped with a liquid nitrogen-cooled radiation shield. The system was cooled by helium passing through the cryostat. The helium temperature and flux was maintained by a thermocouple sensor attached to the retainer. Temperature stability was approximately ±1 K. Films formed at a deposition rate of about $5 \cdot 10^{15} cm^{-2}s^{-1}$ were optically transparent and their thickness d was as great as 10 μm. The high transparency was preserved up to conversion degrees ξ = 0.2—0.25 as monitored with a He—Ne laser (λ = 633 nm) by the absence of changes in the transparency of the reactants and products. At $\xi > 0.7$—0.8 the intensity of transmitted light decreased by 10—25 % in thin ($d \leq 0.5$ μm) and by 30—60 % in thicker films ($d \geq 5$ mm). The changes in optical density in the region of 600—1000 cm^{-1} due to light scattering were less than 0.03 at conversion degree 80—100 %. This variation was taken into account in the IR-band intensity measurements.

Photolysis was carried out in the chlorine dissociative absorption band using a continuous He—Cd laser (λ_1 = 325 nm, absorption cross section $\sigma = 2.5 \cdot 10^{-19}$ cm^2) or N_2 pulsed laser (λ_2 = 337 nm, repetition frequency 1 KHz, $\sigma = 2 \cdot 10^{-19}$ cm^2). The photolysis intensity varied from 10^{14} to $6.5 \cdot 10^{15}$ $cm^{-2}s^{-1}$ using attenuators.

Halogen consumption at the initial stage of the reaction was measured by measuring changes in optical density D at the laser wavelength λ_1, according to techniques described elsewhere.[6] The time resolution was 0.1 s, and the accuracy of the

optical density measurements $\Delta D \sim 4 \cdot 10^{-3}$, which corresponds to the consumption of $28 \cdot 10^{16}$ cm^{-2} Cl_2 molecules in the sample.

Since ethylene and the reaction product, dichloroethane, have well resolved intense IR-bands, the reactant consumption and product accumulation kinetics were monitored by changes in optical density ΔD at the appropriate bands. The absolute values of the absorption cross-sections σ_i of the main characteristic bands of the C_2H_4, C_2H_4:Cl_2 complexes, and of 1,2-$C_2H_4Cl_2$ had been previously measured[6] with an accuracy of 20 %. A two-beam IR spectrometer connected with a computer through an analog-digital converter (ADC) was used in these experiments. The spectrometer was tuned to the maximum of the desired IR-band and its intensity changes were measured in real time on 0.1 s scale. The spectral resolution was 5 cm^{-1}. The accuracy of optical density measurements was $\Delta D = 5 \cdot 10^{-3}$ at time resolution of 1 s, which made it possible to measure the variation of ethylene—chlorine and dichloroethane concentration in the sample $\Delta N_i = \Delta D_i/\sigma_i$ 10^{16} cm^{-2}. The IR spectra detected before and after photolysis had spectral resolution of 1 cm^{-1}. The accuracy of ΔN_i absolute measurements was determined by that of the cross section σ_i. The accuracy of the relative measurements of the conversion degree $\eta(t) = N_r(t)/N_r(0)$ was determined by that of $\Delta(t)$, and amounted to 1—2 %, taking into account the background changes. The error in the measurements of the reaction mean quantum yield and the characteristic time of chain growth depended on sample reproducibility and for a set of 5 similar samples was typically about 20 %.

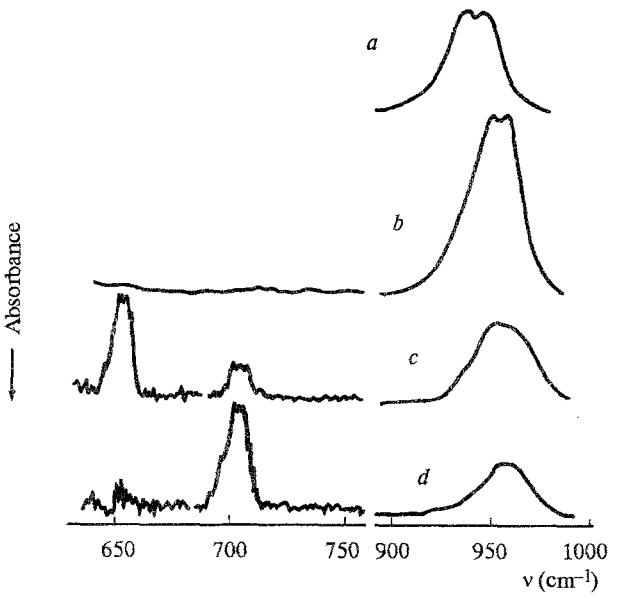

Fig. 2. Infrared spectra of crystalline ethylene (*a*) and chlorine-ethylene binary mixtures before reaction (*b*), after partial conversion via a thermally activated reaction at 90 K for 15 min (*c*) and after brief photolysis at 30 K (*d*). The doublet band at 940—960 cm^{-1} is the ν_7 mode of ethylene. The bands 707 and 653 cm^{-1} are assigned to the C—Cl vibrations of the *trans*- and *gauche*-conformers of 1,2-dichloroethane, respectively.

Results and Discussion

1. IR spectra analysis

In polycrystalline ethylene the most intense IR absorption bands are associated with the out-of-plane bending modes ν_7 (945 cm^{-1}) and ν_{12} (1140 cm^{-1}) which exhibit crystalline splittings.[19—22] In binary mixtures C_2H_4:Cl_2 prepared by deposition from the gas phase the ν_7 and ν_{12} bands are shifted due to formation of donor-acceptor complexes. Absorption spectra in the region the of ν_7 doublet band with maxima at 963 and 955 cm^{-1} are shown in Figure 2.

In triple mixtures (Ar:C_2H_4:Cl_2 = 60:1:1) a broad complex band appears with a maximum at 960 cm^{-1} along with the pure ethylene bands. Heating the triple mixtures above 40 K at a rate of ≈1 K/min causes isolated reactants to combine into complexes that form a crystalline phase, resulting in an increase in doublet band intensity and the simultaneous disappearance of pure ethylene modes. Heating from 35 to 60—65 K is accompanied by intense evaporation of argon (argon vapor pressure at these temperatures[23] is higher than 10^{-4} Torr) and formation of less transparent reactant films presumably because they contain crystals or large aggregates of complexes.

In the absence of illumination thermally activated molecular addition occurs at $T > 85$ K, leading to a decrease in the intensities of the complex bands and the appearance of dichloroethane absorption bands at 653 and 707 cm^{-1}, which are associated with C—C stretching modes of *gauche*- and *trans*-conformers, respectively. The ratio of their intensities shown in Figure 2 indicates that the formation of a thermodynamically unstable *gauche*-conformer dominates under these conditions. The ratio of concentrations of these forms is $N_{tr}/N_g \leq 0.3$. The *gauche*-conformer is converted into the *trans*-form after heating the solid mixture to 110—120 K. In chain photochemical reactions the ratio N_{tr}/N_g is dramatically different (see Fig. 2). The only product is *trans*-dichloroethane. The intensity of the *gauche*-conformer band is below the experimental limit ($N_{tr}/N_g \geq 30$).

The cross sections for dissociative absorption by Cl_2 at λ_1 and λ_2 are several times smaller than those at the main IR-bands of the reactants. For this reason, the kinetic measurements of chlorine consumption were performed in samples 3—10 μm thick with optical density 1—3, while the kinetics of complex consumption was measured in thinner films up to 0.5 μm thick. At the same time, samples 0.5—10 μm thick enable one to detect the accumulation of product.

2. The results of kinetic measurements

Chain reaction kinetics was measured for four types of samples prepared under different conditions:

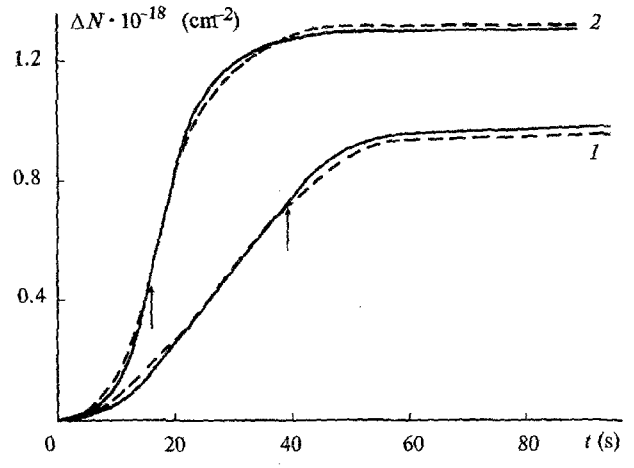

Fig. 3. The kinetic curves of complex consumption (solid lines) and *trans*-dichloroethane accumulation (dashed lines) during photolysis at 30 K (*1*) and 60 K (*2*). The thickness of samples is 10 μm. Light intensity is 10^{15} cm^{-2} s^{-1}. The arrows indicate the time at which photolysis was stopped.

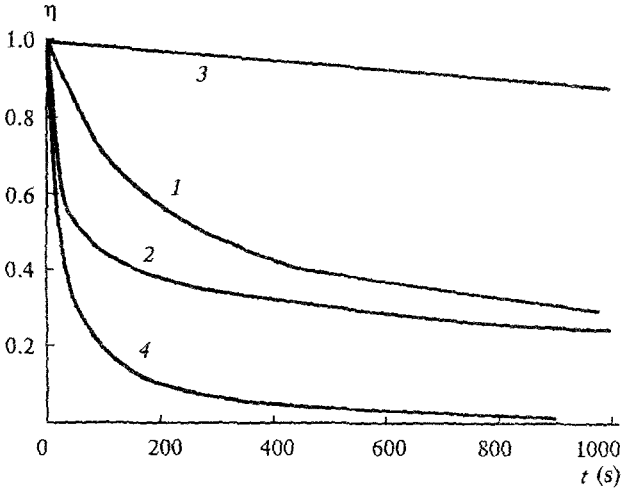

Fig. 4. Kinetics of complex consumption in samples type I, II, III, and IV (curves *1*—*4*, respectively). $I = 3 \cdot 10^{15}$ cm^{-2} s^{-1}, sample thickness is about 0.5 μm. The induction period is not shown.

I. Cl_2:C_2H_4 = 1:1 mixtures prepared by deposition of ethylene and chlorine at T = 23 K.

II. Mixtures of type I after thermal annealing at 60 K.

III. Triple Ar:C_2H_4:Cl_2 = 60:1:1 mixtures.

IV. C_2H_4:Cl_2 = 1:1 mixtures recrystallized by argon evaporation from triple mixtures.

The photolysis in these mixtures results in a decrease both in the intensities of the IR bands of the complexes and in the optical density at the Cl_2 absorption band, and a simultaneous increase in *trans*-dichloroethane IR band intensity. Figure 3 shows Cl_2 consumption and $C_2H_4Cl_2$ accumulation at 30 and 60 K. Kinetic curves have an initial non-stationary period t_0 ~ 5—20 s, where dN_i/dt increases up to a maximum value. At low conversion degrees ($\xi = \Delta N_r/N_r \leq 0.2$) the post-photolysis reaction lasts for 5—20 s because of the slow chain growth. Its kinetics is described by the exponential form: $\Delta N = \Delta N_m[1-\exp(-t/\tau)]$. The characteristic time τ corresponding to chain growth coincides with t_0 during the initial non-stationary photolysis, which is in agreement with the common kinetics of the establishment of a stationary conversion rate.

The photolysis quantum yield at $t > t_0$ is determined by the expression:

$$Y = -\frac{1}{L}\frac{\Delta N_r}{\Delta t} = \frac{1}{L}\frac{\Delta N_p}{\Delta t}$$

where $-\Delta N_r = \Delta N_p$ are the changes in the product and reactant concentrations measured separately, $L = I[1-\exp(-\sigma N_{Cl})]$ is the intensity of the light absorbed by the sample.

Figure 4 shows the photolysis kinetics for each of the four types of samples mentioned above for $t > t_0$. While t and t_0 do not depend on photolysis intensity I, the reaction rate at $t > t_0$ is proportional to I so that Y does not dependend on I and t, but depends on the method of sample preparation as well as on the degree of conversion ξ. Thus binary mixtures with different values of the initial quantum yield $Y(\xi = 0) >> 1$ also differ in $Y(\xi)$ dependences. These dependences at photolysis temperature 30 K for samples of types I, II, and IV are shown in Figure 5. Type IV samples possess the highest $Y(0)$ values equal to ~40, which is 6—7 times greater than $Y(0)$ in type I mixtures. The decrease in Y with ξ in the initial region of the $Y(\xi)$ plot can be characterized by the slope $s_1 = -(dY/d\xi)/Y(0)$ at $\xi = 0$. The values of s_1 for several samples are listed in Table 1.

It is clear that s_1 values for all samples are within the interval of 0.30—0.48, but in mixtures with a high initial $Y(0)$ value, $Y(\xi)$ rapidly decreases when $\xi > 0.3$—0.4, and when $\xi \geq 0.65$—0.75 the yields are approximately the same (Fig. 5). It is worth mentioning that it is possible to obtain 100 % conversion only in samples prepared by argon matrix evaporation (type IV), whereas in samples of types I and II approximately 20—25 % of the reactants are preserved even after long-term photolysis. For this fraction of reactants, $Y < 10^{-2}$. To calculate the kinetic curves for such samples, we determined Y and ξ with respect to the number of reactive complexes.

The temperature dependences of the mean values of $Y(0)$ in binary mixtures are demonstrated in Figure 6. All of the samples have a common feature: the initial quantum yield remains constant from the lowest tem-

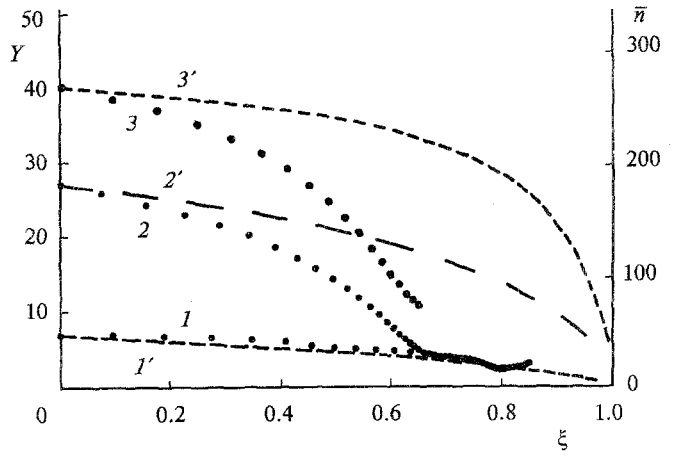

Fig. 5. The dependence of quantum yield (Y) and mean chain length ($\bar{n}$) on conversion degree (ξ). Curves *1—3* relate to samples type I, II, and IV, respectively. Dashed curves are calculated for a $10^3 \times 10^3$ lattice. The number of randomly distributed defects equals $1.2 \cdot 10^4$ (*1'*), $2 \cdot 10^3$ (*2'*) and $8 \cdot 10^2$ (*3'*).

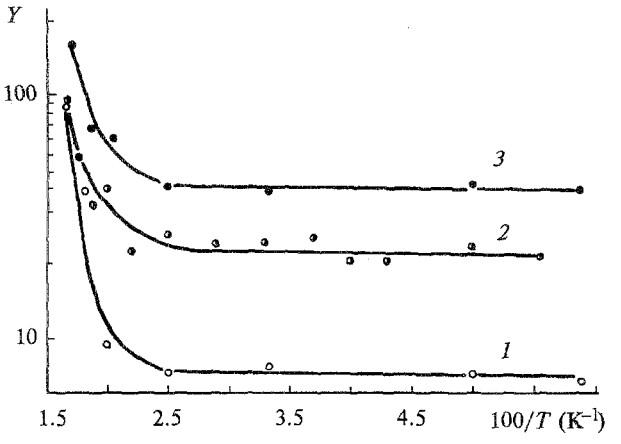

Fig. 6. Temperature dependences of the photolysis quantum yield (Y) in samples type I, II and IV (curves *1—3*, respectively).

perature 17 K up to 45 K. $Y(T)$ increases rapidly in the range 50—60 K. As in the low-temperature region, type IV samples possess the highest Y value, which reaches 160 at 58 K.

High values of $Y >> 1$ mean that the growth of long chains occurs in binary mixtures, chain length being determined by conditions of sample preparation. The quantum yield decreases rapidly with conversion in more perfect samples. In this respect, it should be noted that it is necessary to maintain the temporal and temperature experimental regimes carefully in order to obtain reproducible results.

2.1. Measurements of quantum yield of chain initiation

To determine the quantum yield of chain initiation we carried out the measurements in reactant mixtures diluted by argon (type III), in which only isolated complexes or their small aggregates can be formed. At 60-fold dilution only about 50 % of the complexes are photolyzed. The photolysis quantum yield $Y < 1$ and amounts to 0.3 ± 0.1 in the temperature region 17—33 K. As in binary mixtures, only the *trans*-conformer is formed. At higher dilution, $Ar:C_2H_4:Cl_2 = 120:1:1$, the fraction of complexes converting with the same quantum yield decreases to 25 % while the remaining part has an extremely low quantum yield ($Y < 10^{-2}$).

Halogen atoms are not stabilized in an argon matrix.[24,25] Therefore, chlorine photolysis in triple mixtures occurs only by cage reactions in the complexes, including the consecutive addition of two chlorine atoms formed during photodissociation to one or two adjacent ethylene molecules. If the complexes are spatially isolated in an inert matrix, the chlorine atoms can only react with one ethylene molecule giving mainly the *gauche*-conformer as a result of the cage reactions

$$Cl + C_2H_4 \longrightarrow C_2H_4Cl\,, \qquad (3)$$
$$Cl + C_2H_4Cl \longrightarrow gauche\text{-}C_2H_4Cl_2\,.$$

The quantum yield is determined by competition between these reactions and geminal recombination of halogen atoms, and abstraction of chlorine atoms from the radical:

$$Cl_2 \overset{h\nu}{\rightleftharpoons} Cl + Cl\,, \qquad (4)$$
$$Cl + C_2H_4 \longrightarrow C_2H_4Cl\,, \qquad (5)$$
$$C_2H_4Cl + Cl \longrightarrow C_2H_4 + Cl_2\,.$$

Table 1. Mean values of photolysis quantum yield and s_1 values for samples type I—IV

Sample	T, K	$Y(0)$	s_1
IV	30	40±8	0.30—0.40
IV	58	160±30	0.25—0.35
I	30	7±2	0.35—0.48
II	60	90±20	0.25—0.40
II	30	27±7	0.30—0.45
III	30	0.3±0.1	—

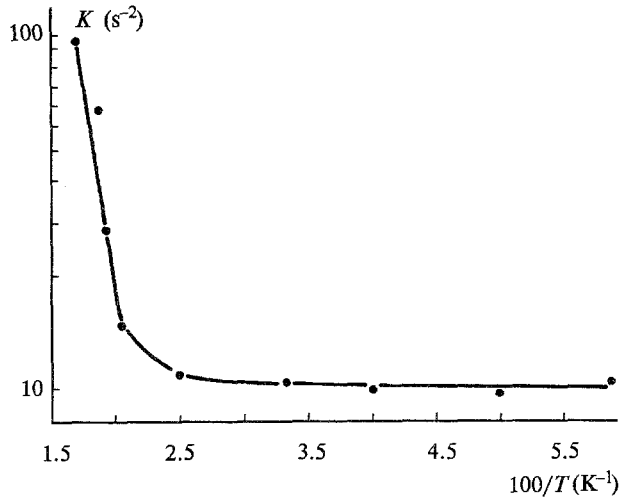

Fig. 7. Temperature dependence of the chain growth rate constant.

The C—Cl fragment of the radical formed in the isolated complex should occupy the place of the chlorine molecule, so that the exoergic reaction of reactant recovery (5) is sterically more favorable than the reaction of *gauche*-conformer formation (3). This reasoning can explain the absence of the *gauche*-conformer and the low quantum yield of the photolysis of the remaining reactants, the fraction of which increases with increasing dilution of complexes.

If complexes are organized into aggregates, the addition of halogen atoms to two different ethylene molecules becomes sterically more favorable, and the two separated radicals initiate chain growth leading to *trans*-dichloroethane. Therefore, the stereospecificity of the reaction is closely connected with the chain mechanism of conversion. The fact that the *trans*-conformer is the only reaction product in triple mixtures demonstrates that conversion mostly occurs in aggregates in which chain length is above 2. According to this line of reasoning, the upper limit of the initiation quantum yield Y_0 can be taken equal to $Y_0 = 0.15$.

2.2 Chain length and effective rate constant.

The mean chain length $\bar{n}$ is determined by the reduced values of Y_0 and $Y(T)$: $\bar{n} = Y(T)/Y_0$, and is 270, 180 and 40 units at $T < 45$ K for samples of types IV, II, and I respectively. At $T = 60$ K, $\bar{n}$ increases to ~ 1000 units. Chain lengths calculated in this way demonstrate that regular structures of complexes of large size (up to 0.5—1.0 μm) are formed in binary mixtures of reactants. In samples prepared by sublimation of the inert matrix (type IV) the size of these structures is 6—7 times greater than in samples obtained by simultaneous deposition of ethylene and chlorine.

It is possible to calculate the effective rate constant of chain growth K_r by using the above values of $\bar{n}$ and the characteristic time of chain growth t, measured in the post-photolysis reaction, viz., $K_r = \bar{n}/t$. The temperature dependence $K_r(T)$ in type II samples is shown in Figure 7 and is characterized by a low temperature plateau below 40 K where K_r 10 s^{-1} . Above 50 K, K_r increases with activation energy E_a = 1 kcal/mol. By measuring t in different samples one finds that t is proportional to $Y(0)$, so that the rate constant for chain growth does not depend on sample preparation conditions, at least at the initial stage of photolysis.

3. Computer simulations of chain growth

The computer simulation of chain growth in a mixed C_2H_4:Cl_2 crystal was performed using the algorithm proposed in ref. 17, with the following stages:

1. the calculation of lattice parameters;
2. determination of the equilibrium configuration of the reactants in the crystal;
3. calculation of the PES (potential energy surface) and the transition probability using the multidimensional dynamic nuclear tunneling model.

The crystal energy was calculated from the pair interaction of chemically uncoupled atoms, described by the Buckingham potential:

$$U(r) = -M/r^6 + N \cdot \exp(-q \cdot r) , \qquad (6)$$

with interaction constants given in Table 2. The mutual arrangement of molecules in a C_2H_4:Cl_2 complex was selected in accordance with quantum chemical calculations[27—29]: the distance between the nearest Cl atom and the C = C plane of ethylene was r_0 ~ 3.0—3.2 Å, which is 0.4—0.6 Å shorter than the equilibrium van-der-Waals distance. This shortening is due to the charge transfer in the donor—acceptor complex. In our calculations we selected effective charges $\pm q$ (q = 0.19 e) located on the carbon and chlorine atoms in order to obtain the aforementioned r_0 values and the experimen-

Table 2. Parameters of atom—atom potentials (ref.[27]).

Atoms	M, $\frac{\text{kcal}}{\text{mol}}$ Å^6	N, $\frac{\text{kcal}}{\text{mol}}$	q, Å^{-1}	r_0, Å
Cl—Cl	2900	$2.29 \cdot 10^5$	3.513	3.696
Cl—C	1420	$1.13 \cdot 10^5$	3.513	3.701
Cl—H	456	$1.05 \cdot 10^5$	4.194	3.100
C—C	476	$3.77 \cdot 10^4$	3.513	3.698
C—H	155	$3.28 \cdot 10^4$	4.130	3.152
H—H	40.1	$2.86 \cdot 10^4$	5.200	2.433

tal[28] value of complex binding energy of 6 kcal mol^{-1}. Therefore, the intermolecular interaction energy was determined as the sum of atom—atom potentials (6) and Coulomb interaction. Crystal parameters were calculated by minimization of the intermolecular interaction energy by varying the elementary lattice cell dimensions (a, b, c), crystallographic Euler angles (α, β, γ) and orientation of the complex as a whole in the cell. In addition, the crystallographic parameters of the lattice depend on the type of symmetry, which in the case of C_2H_4:Cl_2 = 1:1 crystals is unknown. As the initial structure we have chosen[17] a simple triclinic P_1-type lattice with one complex C_2H_4:Cl_2 in each unit cell (Z = 1). However, the great chain lengths and high conversion degree observed in the experiment indicate that the reactant and product lattices must belong to the same symmetry group. We recalculated all the parameters of the ethylene—chlorine crystal with a monoclinic lattice P_21/C (Z = 2), which has the same symmetry as that of dichloroethane and contains two complexes in each unit cell, distanced at a half-period along the (010) axis and a half-period along the (100) axis with respect to each other. To test the optimization method and adequacy of the atom—atom potential, the dichloroethane crystal lattice was calculated, and it gave lattice parameters agreeing with experimental data within an error of less than 0.2 Å (Table 3).

The results of calculations for the P_1 and P_21/C lattices are also presented. A characteristic feature of the obtained lattices is that the molecules lie nearly in the ac-plane (Figure 1, where ethylene displacement out of this plane does not exceed 2°), so that the crystals possess relatively weak inter-plane interaction compared to intra-plane interaction.

A comparison of the calculated isomorphic lattices of the reactant and product crystals shows their commensurability in the reaction plane ac. Nevertheless, the inter-plane distance of the reactant lattice is 0.3—0.4 Å greater than that of the products. Yet, the PES has the flattest minimum in this direction, compared with others, and it is impossible to say definitely whether this difference actually takes place. Taking into account this uncertainty and the fact that the reactant and product crystals have a quasi-two-dimensional structure, the following simulations were carried out only in the ac-plane.

3.1 Determination of the equilibrium configuration of reactants in a crystal

Photolysis of chlorine results in the creation of a pair of C_2H_4Cl radicals, which disturb[3] the environmental region in a crystal. The minimization of the intermolecular interaction energy in the vicinity of the radicals shows that molecules which belong to the second and the third coordination spheres do not undergo significant displacement and their positions can be assumed to be fixed. A radical and the adjacent chlorine molecule form a reactive pair in which the distance between interacting C and Cl atoms is essentially shorter ($R_1 \approx 3.2$ Å) than the van-der-Waals equilibrium distance 3.65 Å (see Figure 1*a*). The reaction barrier height, as will be discussed below, is 2 kcal mol^{-1}. The lack of free volume is caused mainly by the disappearance of a donor—acceptor complex. This brings about deformations along the small diagonal of the ac-plane, which provides the proper conditions for formation of *trans*-dichloroethane and a chlorine atom. The latter quickly reacts with the ethylene molecule and forms a radical in the next lattice site, giving rise to another link of chain growth along the same direction. It is worth mentioning that the chain grows symmetrically in two directions (see Figure 1b). In the process of chain growth dichloroethane molecules subsequently replace ethylene molecules in lattice sites. Nevertheless, reaction product formation does not induce large changes in the equilibrium configuration of the reaction complex: R_1 and the reaction barrier height change less than 0.2 Å and 0.2 kcal mol^{-1}, respectively.

The distance R_2 from the C atom of the radical to the nearest Cl atom of a molecule situated at the neighboring small diagonal of the ac-plane equals 3.75—3.8 Å and far exceeds R_1. The reaction barrier corresponding to R_2 reaches 5 kcal/mol, which rules out the chain transition to the neighboring diagonal and indicates linear propagation of isolated chains. It is noteworthy that product formation does not lead to changes in the lattice period or to the appearance of structural defects associated with the incommensurability of reactant and product lattices. The linear chain propagation considered above is analogous to the high-temperature polymerization of diacetylenes.[30] However, the fundamental difference between the two processes is that polymer growth causes significant changes in the period

Table 3. Parameters of the reactant and product crystal lattices.

Parameters of the crystal	Calculated crystal			Crystal**
	C_2H_4:Cl_2		$C_2Cl_2H_4$	$C_2Cl_2H_4$
	triclinic Z = 1	monoclinic Z = 2	monoclinic Z = 2	monoclinic Z = 2
a	4.31	4.31	4.55	4.66
b	4.10	5.20*	4.83*	4.78*
c	7.55	7.55	7.60	7.88
α	90°	90°	90°	90°
β	95°	95°	95°	103°
γ	120°	140°	142°	145°

*To compare b and γ for triclinic (Z = 1) and monoclinic (Z = 2) lattices, these parameters are identified with the distance between non-equivalent molecules and the angle between the ac-plane and the b vector, respectively.
**Data from ref.33.

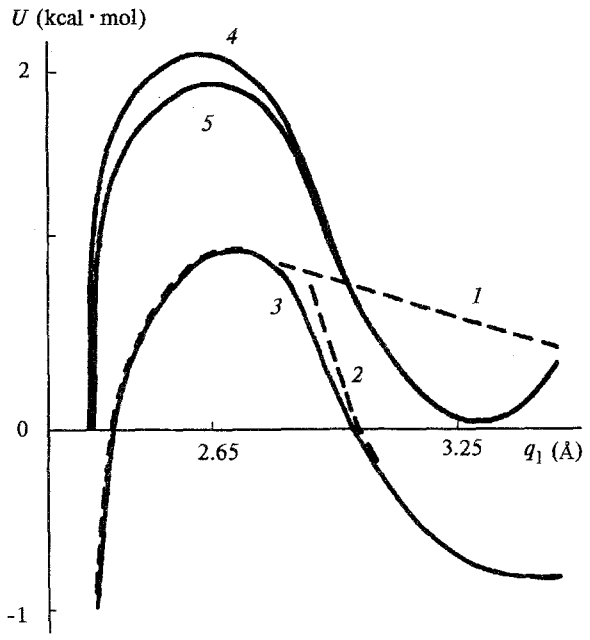

Fig. 8. Potential energy of interaction between a radical and a chlorine molecule calculated using LEPS (*1*), using atom-atom potentials (*2*), approximate composite surface from *1* and *2* (*3*), in a crystal without environmental reorganization (*4*) and with reorganization (*5*). Cl—Cl distance equals 1.99 Å.

of reactant and product arrangement (that is, polymer shrinkage) even at a comparatively high degree of commensurability of monomer and oligomer unit lattices (the difference is less than 0.2 Å). This leads to a subsequent increase in the reaction barrier height during chain growth, and, finally, to its termination.

The chain growth mechanism changes when a radical pair is created near product molecule (Fig. 1c). Since dichloroethane molecules displace the adjacent chlorine molecules from the small diagonal, the equivalence of the two opposite directions of chain growth becomes broken. The barrier height and the value of R_1 for the radical driving chain growth to the right in Figure 1c, are practically the same as for growth of an isolated chain. For the second radical already at the first step R_1 equals 3.45 Å, and the barrier height reaches 3.4 kcal/mol, which makes one-side propagation preferable. Another peculiarity of chain growth is the considerable shortening of the distance R_2 between the radical and the chlorine molecule placed on the neighboring diagonal, R_2 = 3.5—3.55 Å; the barrier height decreases to 3 kcal/mol. As will be shown below, the reaction with this Cl_2 molecule (resulting in *trans*-dichloroethane) can compete with linear chain propagation and can lead to a «kink», that is, a skip of the chain to the neighboring diagonal.

In concluding this section let us note the three results which are important for understanding the mechanism of chain growth. First, reactants in the initial state are placed at distances shorter than the van-der-Waals distances which reduces the reaction barrier height. Second, commensurability of the reactant and product lattices favors the growth of an isolated linear chain in two opposite directions. Third, when active centers are produced in the vicinity of the product molecules, one-sided chain propagation becomes more probable and kinks can appear.

3.2 Calculation of the PES and the reaction rate constant

PES calculations at short distances were made with the semiempirical LEPS method,[31] where singlet $U^1{}_{\alpha\beta}$ and triplet $U^3{}_{\alpha\beta}$ energy states are described as Morse and anti-Morse functions for the (Cl—Cl) bond which is cleaved, and the (C—Cl) bond, which is formed. According to the method proposed by Sato,[32] the Coulomb (Q), and exchange (J) integrals are defined as

$$Q_{\alpha\beta} + J_{\alpha\beta} = (1 + s^2) \cdot U^1{}_{\alpha\beta}, \qquad (7)$$
$$Q_{\alpha\beta} - J_{\alpha\beta} = (1 - s^2) \cdot U^3{}_{\alpha\beta},$$

and the energy of the three-particle complex C—Cl—Cl is given by

$$U = \frac{1}{1+s^2}\left[Q_{\alpha\beta} + Q_{\beta\gamma} + Q_{\alpha\gamma} - \left\{\frac{1}{2}\left[(J_{\alpha\beta} - J_{\beta\gamma})^2 + (J_{\beta\gamma} - J_{\alpha\gamma})^2 + (J_{\alpha\gamma} - J_{\alpha\beta})^2\right]\right\}^{1/2}\right] \qquad (8)$$

The adjustable parameter s is the overlap integral and it is selected so that it provides saddle point energy equal to the experimental gas-phase reaction activation energy. Since this method does not take into account long-range dispersion interactions mainly determining the equilibrium distances between the reactants, the potential energy surfaces in the far region were approximated by atom—atom potentials, as shown in Figure 8.

In the PES computation the displacements of the reactants and the neighboring environment were found by minimization of the potential energy at fixed C—Cl distances.

The two-dimensional PES as a function of the coordinates of the Cl—Cl bond which is cleaved, (q_1), and the C—Cl bond which is formed (q_2), is plotted in Figure 9. It is an «early descent» PES, that is, the saddle point is strongly shifted towards the reactants valley, so that the reaction barrier is overcome practically without lengthening of the bond to be broken. The extremal trajectory of multidimensional nuclear tunneling is determined by the ratio of the longitudinal vibration fre-

quency in the initial state $\omega_{\parallel}$ to the transverse vibrational frequency $\omega_{\perp}$ as well as by the angle φ between the reactant and product valleys. For the considered reaction $\omega_{\parallel} = 75$ cm^{-1}, $\omega_{\perp} = 570$ cm^{-1} and $\varphi \approx 90°$, so that

$$\omega_{\parallel}/\omega_{\perp} << 1. \qquad (9)$$

Inequality (9) means that the extremal trajectory corresponds to a slow-flip (vibrational-adiabatic) transition[34] and coincides with the minimum energy path (MEP) passing through the saddle point, unlike the «cutting corner» trajectories of hydrogen transfer between heavy fragments.[35–37]

Sections of the MEP for different equilibrium configurations of the reactants are shown in Figure 10. The barrier height is determined by the initial distance between the reactants, as well as by the character of their motion. The important role of intermolecular the $C_2H_4Cl—Cl_2$ stretching vibration and the C—C—Cl bending vibration for the reaction in question has been elucidated in ref. 17. We consider below the dynamic behavior of the reactants, taking into account contributions from the other vibrations as well.

3.3. Dynamics of reactant vibrations in the crystal

Analysis of the reactants' motion along the MEP shows that the displacement of the reactants' center of mass is smaller than that along the reaction path. The reorganization energy of the medium equals 0.12—0.17 kcal/mol and is considerably less than the reaction barrier height. Based on this fact, we considered the dynamic problem of reactant vibrations in the complex Cl—Cl...C—C—Cl immersed in a fixed crystalline environment, thus neglecting the low-frequency lattice vibrations. Since the crystal *ac*-planes interact weakly with each other, we considered the reactant motions

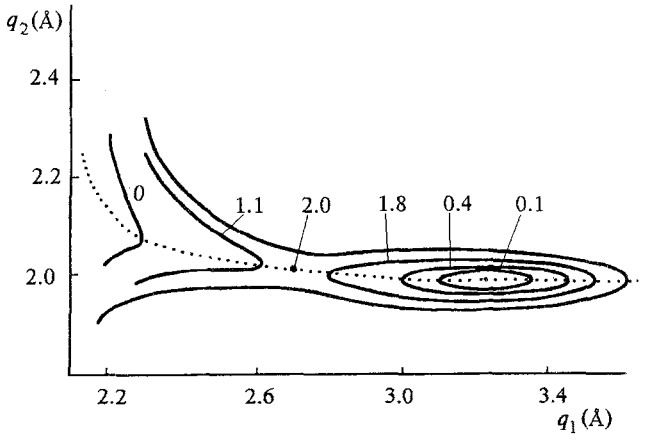

Fig. 9. Two-dimensional PES in q_1,q_2 coordinates.

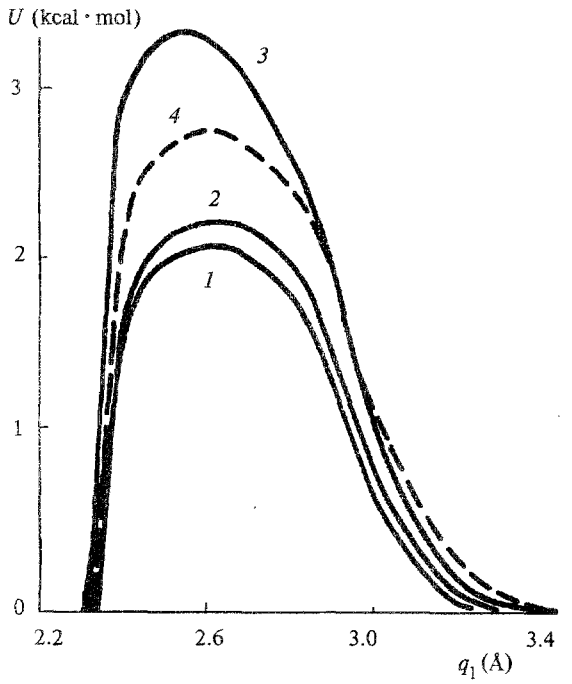

Fig. 10. PES section along the MEP for different initial reactant configurations. *1*, Isolated chain growth at $R_1 = 3.25$ Å (see Fig. 1*b*); chain growth in the vicinity of the reaction product line (see Fig. 1*c*); *2*, chain growth to the right at $R_1 = 3.3$ Å; *3*, the same to the left at $R_1 = 3.45$ Å; 4, reaction with the molecule located on the adjacent diagonal at $R_2 = 3.5$ Å (kink).

only in this plane using a space of 7 inter- and intramolecular coordinates. The changes in the lengths and angles of the bonds were chosen as natural coordinates q_i. After transforming to normal coordinates Q_i, the vibrational frequencies ν_i shown in Table 4 were obtained.

The three high-frequency vibrations assigned to the stretching modes of the chlorine molecule and the radical practically do not mix with the other modes. The Q_7 vibration with intermediate frequency value is mainly due to bending vibration in the radical. The low-frequency vibrations $Q_4—Q_6$, possessing the largest zero-point amplitudes, are intermolecular stretching (Q_4 and Q_5) and librational (Q_6) motions.

The kinematics of the low-frequency vibrations is shown in Figure 11. The $Q_1—Q_3$ coordinates are essentially constant up to the saddle point and make little contribution to the reaction coordinate.

In Figure 12 the changes in the other four coordinates along the reaction path s are presented for the equilibrium reactant configuration shown in Figure 1*a*. The main contributions come from the Q_5 and Q_6 vibrations which corresponds to the simultaneous ap-

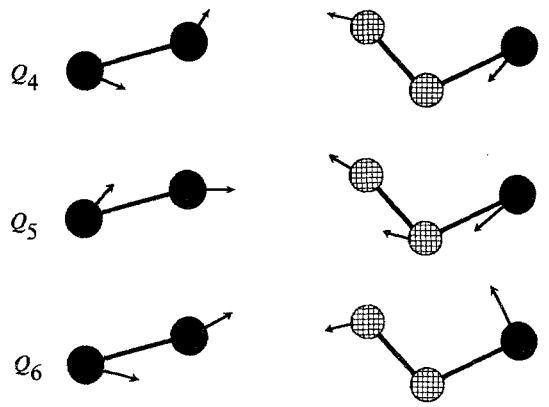

Fig. 11. Kinematics of normal vibrations Q_4, Q_5 and Q_6 of the planar reaction complex Cl—Cl...C—C—Cl.

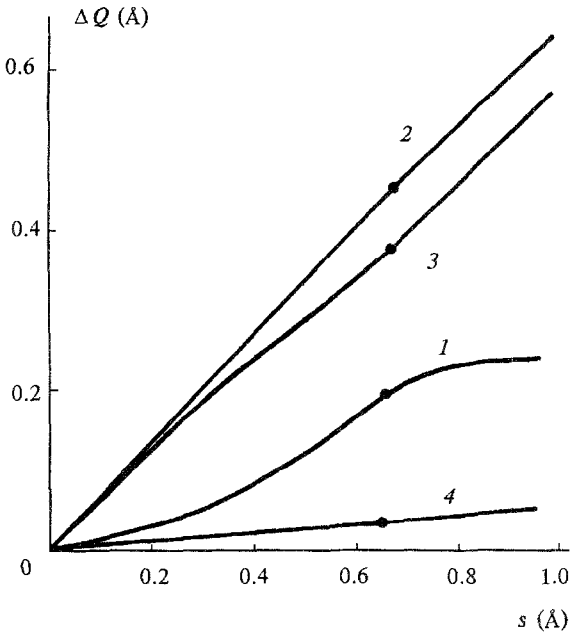

Fig. 12. Variations of the normal coordinates Q_4 (*1*), Q_5 (*2*), Q_6 (*3*) and Q_7 (*4*) along the reaction path *s*. Asterisks denote the saddle point.

proach and rotation of the reacting particles.

In the other reactant equilibrium configurations considered the vibrations Q_5—Q_7 contribute to the reaction coordinate in a different way. For example, when chain growth occurs near the product (Fig. 1*a*), the reactant motion leading to chain propagation to the right is similar to that considered above. However, for the reaction of the C_2H_4Cl radical the contribution from the vibration Q_6 decreases, while that from the rigid mode Q_4 rises, which leads to a sharp increase in the reaction barrier height and to the aforementioned of the alternation chain growth. On the other hand, in the reaction of the first radical with the Cl_2 molecule the role of librational vibrations Q_5 and Q_6 rises, resulting in a relatively low barrier height even at large equilibrium distance $R_2 \approx 3.50$—3.55 Å (see Fig. 10).

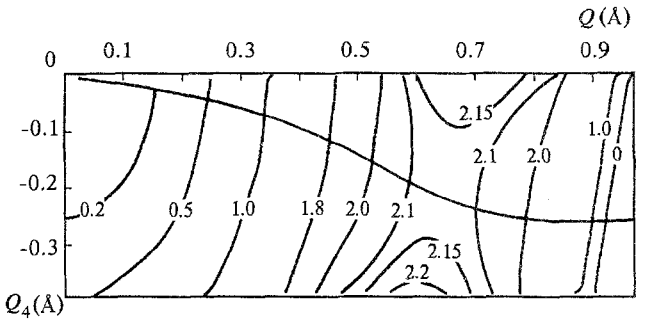

Fig. 13. Two-dimensional PES in Q, Q_4 coordinates.

Table 4. Frequencies of in-plane normal vibrational modes of the Cl—Cl...C—C—Cl reaction complex

Coordinates	ν_i, cm^{-1}	Zero-point amplitude*, Å	Assignment	
Q_1	568	0.027	Cl—Cl	Stretching
Q_2	899	0.001	C—Cl	
Q_3	1872	0.011	C—C	
Q_4	64	0.027		Intermolecular liberation and bending modes
Q_5	74	0.077		
Q_6	101	0.085		
Q_7	361	0.072	C—C—Cl	Bending

*Projection of the zero-point amplitude on the reaction coordinate.

3.4. Calculation of the rate constant for the chain

The coordinates Q_1—Q_3 are perpendicular to the reaction path s. As follows from Figure 12, the motion in space of the slow coordinates Q_4—Q_7 is characterized by a nearly linear change in Q_5—Q_7 with *s*. It turned out that it was possible to define a new coordinate

$$Q(s) = \sum_{i=5}^{7} \lambda_i Q_i(s)$$

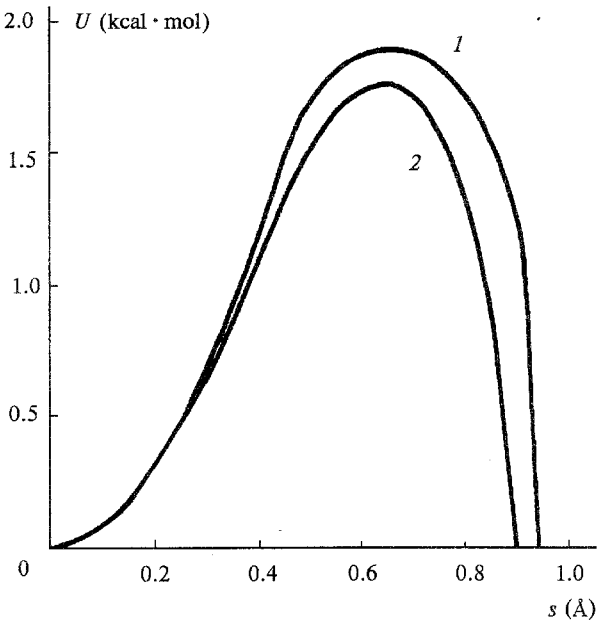

Fig. 14. PES section along the reaction path (*1*) and the vibrationally adiabatic potential (*2*).

as a linear combination of Q_5-Q_7 so that the MEP trajectory lies completely in the Q,Q_4-plane. This permitted us to reduce the dimensionality of the 4-D PES to two dimensions (see Figure 13). Motion along the reaction coordinate is adiabatic with respect to the fast coordinates (since $\omega_{\parallel} << \omega(Q_1)$, $\omega(Q_2)$, $\omega(Q_3)$, which corresponds to condition (9)) and non-adiabatic in the space of the slow coordinates Q_4-Q_7, as follows from Figure 13 ($\omega_{\parallel} >> \omega_{\perp}$). Nevertheless, since the MEP is nearly a straight line, deviation of the extremal trajectory from the MEP is small. The barrier along the straight-line path increases by only 0.1 kcal mol^{-1}, and the path itself s is shortened by only 0.03 Å. Thus the MEP was chosen as the extremal trajectory in further calculations.

The vibrationally-adiabatic potential and $V(s)$ are shown in Figure 14. The barrier height for the zero-point vibrational level of the initial state equals 1.8 kcal/mol and the effective tunneling length is 0.8 Å. The effective mass of a tunneling particle is found from the relation

$$V(s) = \frac{m}{2}\omega^2 s^2 \qquad (10)$$

and equals 24.8 a.u., which is significantly less than the reactants' reduced mass (32.4 a.u.) due to the participation of intermolecular librational and bending vibrations in the tunneling transition.

In view of the adiabaticity of the motion with respect to the fast transverse coordinates it is possible to use the vibrationally-adiabatic potential[38]:

$$V_{ad}(s) = V(s) + \frac{h}{2}\sum_i \Delta\omega_{\perp i}(s) \qquad (11)$$

where $\Delta\omega_{\perp i}$ are the changes in frequencies of the transverse vibrations Q_1-Q_3 and of two linear combinations of Q_4-Q_6 which appeared after the aforementioned reduction of the PES. The calculated potential $V_{ad}(s)$ was approximated by a cubic parabola in order to simplify the calculations :

$$V_{ad}(s) = \frac{1}{2}m\omega^2 s^2 - \frac{1}{6}m\lambda s^3 . \qquad (12)$$

The energy values of the metastable state are complex

$$E_n = E^0{}_n - i\Gamma_n/2, \qquad (13)$$

and correspond to the poles of the quasiclassical spectral function[39]

$$g(E) \propto \sum_{\text{period}} \exp(i(W(E) - l\pi/2)) \qquad (14)$$

where the action is $W(E) = \oint p dx$, and l is the number of turning points along the trajectory.

The period of a classical trajectory in a well is

$$\tau_{1n} = 2\int_{s_1'}^{s_1} ds(2m(E_n - V(s))^{-1})^{1/2} \qquad (15)$$

and the action

$$W_{1n} = \frac{2}{\hbar}\int_{s_1'}^{s_1} ds(2m(E_n - V(s)))^{1/2} \qquad (16)$$

where s_1 and s_1' — are the turning points in the well. In addition, there exist the trajectories with an imaginary period corresponding to tunneling through the barrier from s_1 to s_2:

$$i\tau_{2n} = 2\int_{s_1}^{s_2} ds(2m(E_n - V(s))^{-1})^{1/2} \qquad (17)$$

$$iW_{2n} = \int_{s_1'}^{s_1} ds(2m(E_n - V(s)))^{1/2} \qquad (18)$$

Therefore, an arbitrary periodic orbit has a complex period $\tau_{nm}(E) = n\tau_1(E) + im\tau_2(E)$ and the action $nW_1(E) + imW_2(E)$. Direct summation over all of the periodic orbits leads to the expression for the spectral density

$$g(E) = \propto \frac{\exp(i(W_1 - \pi)) + \exp(-W_2)}{1 - \exp(i(W_1 - \pi)) - \exp(-W_2)} \qquad (19)$$

Thus, the quantization rule is

$$1-\exp(iW_1-\pi)-\exp(-W_2) = 0. \qquad (20)$$

Since $\exp(-W_2) << 1$, as a zero approximation one obtains from this equation the usual Bohr-Sommerfeld quantization condition

$$W_1(e) = 2\pi\left(n+\frac{1}{2}\right) \qquad (21)$$

and, to the first order, the width of the level

$$\Gamma_n = \frac{1}{\tau_n^1(E_n^0)}\exp(-W_2(E_n^0)) \qquad (22)$$

We have found six energy levels in the initial state for potential $V(s)$: $E^0_0 = 0.16$, $E^0_1 = 0.50$, $E^0_2 = 0.81$, $E^0_3 = 1.12$, $E^0_4 = 1.41$, $E^0_5 = 1.67$ kcal/mol. All the levels obey $\Gamma_n << E^0_n$. The spectrum was assumed be continuous above the upper energy level because the width Γ_5 is comparable to $V_0-E^0_5$, where V_0 is the barrier height. Assuming the Gibbs equilibrium population of the levels in the initial well one obtains the following expression for the transition probability

$$W(T) = \left(\sum_{n=0}^{5} \exp\left(-\frac{E_n^0}{kT} - \frac{2}{\hbar}S(E_n^0)\right) + \right.$$

$$\left. + \int_{E_5^0}^{\infty} dE \frac{\exp(-E/kT)}{1+\exp(-2\pi/\hbar\omega(E-V_0))} \right) Z_0^{-1} \qquad (23)$$

where Z_0 is the partition function for the initial well.

The temperature dependence $W(T)$ calculated from (23) is given in Figure 15. It is characterized by a low-temperature plateau with a sharp transition to the Arrhenius region (at T_c = 20—25 K) with an activation energy 1.4 kcal/mol above T_c, in agreement with the experimental data. The value of the reaction rate constant in the region of the low temperature plateau, $K_0 = 10^{-2}$—10^{-1} s^{-1}, is 2—3 orders smaller than the experimental value. This discrepancy in K_0 and T_c is within the accuracy of the calculations. Notice that when the barrier height increases to 3.5 kcal/mol, the value of K_0 decreases by five orders of magnitude, so that this is the limiting value for low-temperature reactions of this type.

The present consideration does not claim to reproduce the experimental data quantitatively, but it does describe many of salient characteristics of low-temperature chemical reactions involving heavy particles, namely:

1. The local lattice deformations created during reaction initiation and chain propagation, induce close packing of the reaction complex, in which the distances between the reactants are shorter than the equilibrium van-der-Waals distances. This results in a decrease in both the height and width of the potential barrier.

2. The reaction is characterized by an «early descent» type of PES and vibrationally adiabatic motion along the MEP.

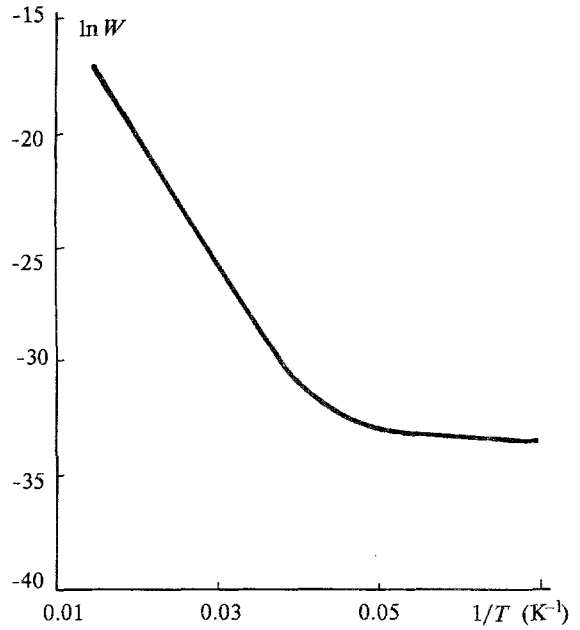

Fig. 15. Temperature dependence of the tunneling transition probability.

3. This motion is determined by a set of intermolecular reactant vibrations whose zero-point amplitudes are considerably greater than those of the intramolecular vibrations.

4. Participation of intermolecular libration and bending vibrations in the motion along the reaction coordinate leads to a decrease in the barrier height and in the effective mass of a tunneling particle.

5. The temperature dependence $K(T)$ is characterized by a sharp transition from the Arrhenius curve to a low-temperature plateau.

6. The lattice deformation accompanying accumulation of the product causes spatial correlations of chain growth. These correlations directly influence the chain growth rate constant, and, hence, may lead to alternation of the chain growth or radical stabilization, as well as to changes in the direction of the chain growth.

Within the framework of these conclusions, we now present an analysis of some of kinetic peculiarities of the chain reaction given in the experimental part of the paper.

4. Spatially correlated chain growth

The kinetics of unbranched chain chemical reactions is characterized by temporal and spatial correlations,

which are due to interactions of individual chains. Thus, the photolysis kinetics of an optically thin sample is described by:

$$\eta = \frac{k_0^2 - k_1\sigma I}{k_0^2 - 2k_1\sigma I} e^{-\bar{n}\tau} - \frac{k_1\sigma I}{k_0^2 - 2k_1\sigma I} e^{-k_0 t} \qquad (24)$$

where $\tau = \sigma It$, $\sigma = \sigma_1 Y_0$, k_0 and k_1 are the constants of chain termination and growth, respectively,

$\bar{n} = k_1/k_0 + 1 >> 1$

is the chain length. The second term in (24) determines the induction period $t_0 \sim k_0^{-1}$ at low initial reaction rates, whereas the first one describes the following growth of the chain at quasistationary concentration of active centers. If

$$2\ \bar{n}\ \sigma I << k_0 \qquad (25)$$

the growth of a new chain begins after termination of the previous chain in the volume $\bar{n}\ a^3_0$ (a^3_0 is the molecular volume), and the reaction kinetics is given by

$$\eta = \exp(-\bar{n}\,\tau), \qquad (26)$$

so that condition (25) means that temporal correlations are absent. In regular structures each chain terminates when its active center meets a lattice defect or a reaction product. When the lattice defects and initiation sites are randomly distributed, the growth of chains with different lengths can be characterized by the distribution function $P(n)$ such that

$$\eta(\tau) = \int P(n,\tau)dn\,. \qquad (27)$$

For independent quasistationary growth the initial distribution function $P(n,0)$ changes exponentially with time, and the dependence $\eta(\tau)$ is the inverse Laplace transform of $P(n,0)$:

$$\eta(\tau) = \int P(n,0)e^{-n\tau}dn\,. \qquad (28)$$

The spatial correlations of the chains change the distribution function P(n, τ), which can be described by the master equation

$$\frac{dP(n,\tau)}{d\tau} = -nP(n,\tau) - k_n P(n,\tau) + \int k_{n,n'}P(n',\tau)dn \qquad (29)$$

where $k_n P(n, \tau)$ is the rate of escape from the configuration of length n into other configurations, and $k_{n,n'}$ is the rate of reverse transitions. Integration of (29) gives a more general equation

$$d\eta / d\tau = -\int nP(n',\tau)d\tau\,. \qquad (30)$$

Relations (28) and (30) give the main equation for the analysis of the kinetic curves,

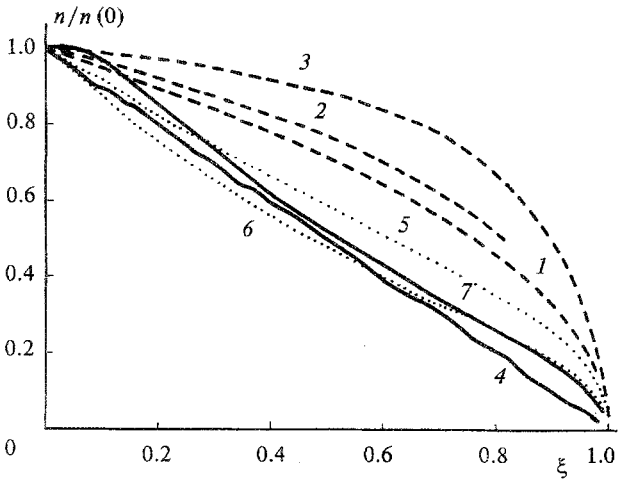

Fig. 16. Calculated dependences of the mean chain length on the conversion degree (ξ) in a $10^2 \times 10^2$ lattice for double-sided propagation (dashed lines) at different concentrations of defects ($N_d >> 1$ (*1*), $N_d = 3$ (*2*), $N_d = 1$ (*3*)); for single-side propagation at $N_d = 0$ (solid line 4); when kinks are formed (dotted lines), at $N_d = 3$ and $P_y = 0.04$ (*5*), $P_y = 0.1$ (*6*), $P_y = 0.2$ (*7*).

$$\bar{n} = -\frac{1}{\eta}\left(\frac{d\eta}{d\tau}\right) = -\frac{\int nP(n,\tau)dn}{\int P(n,\tau)dn} \qquad (31)$$

This equation merely expresses the law of conservation law of the total number of active particles and is not based on any model. It shows that the mean chain length is equal to the first momentum of a distribution function, and, in the absence of time correlations, depends only on the conversion degree. It is possible to expand $\bar{n}$ (ξ) into a series in the distribution function momenta $M_k = \int n^k P(n,\xi)dn$, viz.,

$$\bar{n}\,(\xi)/\bar{n}\,(0) = 1 - s_1\xi + O(\xi^2) \qquad (32)$$

where $s_1 = (M_2 - M_1^2)/M_1^2$ characterizes the distribution function dispersion and determines the rate at which $\bar{n}(\xi)$ changes.

Expressions (31) and (32) provide a means for determining the effect of spatial correlations on $\bar{n}(\xi)$. A computer simulation was carried out on a two-dimensional $N \cdot N$ lattice ($N = 10^3$). It was assumed that a chain grows along the X-axis until it encounters a defect, product, or crystal surface. If the chain is allowed to grow in two opposite directions the chain length is determined by the distance between two random defects. When the average number of defects N_d per one initial line of length N is such that

$N >> N_d >> 1$, the initial distribution function is

$$P(n,0) \approx \frac{1}{\bar{n}_0^2} n e^{-n/\bar{n}_0}, \ \bar{n}_0 = N / N_d \qquad (33)$$

so that

$$\bar{n}(\xi)/\bar{n}_0 = (1-\xi)^{1/2}, \ s_1 = 0.5. \qquad (34)$$

At lower defect concentrations the value of s_1 decreases, and the change in $\bar{n}(\xi)$ is slower than that predicted by (34), tending to $\bar{n}(\xi) = N$ at $N_d = 0$, as shown in Figure 16.

In the case of one-side propagation, a chain of length n in a segment of length X between defects leads to a decrease in the available length for next chain growth to X–n. The distribution function can be approximated by:

$$P(n,0) = \frac{1}{\bar{n}_0} e^{-n/\bar{n}_0} \qquad (35)$$

so that

$$\bar{n}(\xi)/\bar{n}_0 = 1-\xi, \ s_1 = 1. \qquad (36)$$

The experimental curves $\bar{n}(\xi)$ shown in Figure 5 clearly do not obey the relation (36). Therefore, one can conclude that there is two-sided chain propagation. Type I samples satisfy equation (36). This confirms the assumption that the growth of short chains is not disturbed by spatial correlations and is generally governed by the concentration of defects. This situation changes in samples II and IV. On the one hand, the lower s_1 values prove lower defect concentration, but on the other hand, the sharp decrease in $\bar{n}(\xi)$ at $\xi > 0.3$ shows that there are additional mechanisms leading to chain breakage during conversion. According to the geometry of chain growth considered in the previous section, the non-equivalence of chain growth in two directions and the formation of kinks can lead to the effects mentioned above. The $\bar{n}(\xi)$ dependence connected with the formation of kinks differs from that corresponding to one-sided propagation. A kink can only appear if along with the probability P_x of chain growth in the X direction, there is a finite probability P_y that the active center will react with the molecule at the neighboring line. A kink only appears at $n > P_x/P_y$, so that at high degrees of conversion the chain length is limited by defects, as is the case for $P_y = 0$. The calculated curves $n(\xi)$ at different P_y are given in Figure 16. The inequality $P_y << 0.05$ corresponds to experimental values s_1 0.35. In addition, $\bar{n}_0$ decreases at high P_y values. Although it is possible to select s_1 to be in agreement with the experimental data at $P_y < 0.05$, the simulated curves do not explain the relatively sharp decrease in $\bar{n}(\xi)$ at $\xi > 0.3$ typical of the type IV and II samples.

Therefore, according to the results of section 3.1, one can assume that the probability of kink formation increases with accumulation of the product. The $\bar{n}(\xi)$ dependence when P_y is proportional to ξ, which is shown in Figure 16 (curve 7), fits the experimental data better. The s_1 value at the initial stage of the reaction is determined by the concentration of defects, and, as the product is accumulated, the chain length sharply decreases and eventually a short chain growth regime comes about, as in the type I samples .

Thus, the comparison of the calculated chain growth geometry with the kinetic data shows that the activationless growth of long chains and the high degree of conversion in this reaction take place due to three factors: regular arrangement of the reactants, high probability of tunneling transition, and commensurability of the reactant and product lattices. The maximum chain length is determined by the concentration of defects in a sample, while the spatial correlations, which are due to accumulation of the product, lead to a decrease in the chain length during conversion.

The increase in $\bar{n}_0$ with increasing T at $T > 45$ K (Fig. 6) can be explained by a decrease in the effective defect concentration. The decrease in s_1 to 0.25–0.3 at high temperatures supports this conclusion. In annealed samples (types II and IV) the increase in $\bar{n}(T)$ is probably connected with thermally activated surmounting of the reaction barrier in the vicinity of a structural defect. The sharper dependence of $\bar{n}(T)$ in defective samples (of type I) is probably associated with additional annealing of non-equilibrium defects.

* * *

The consideration presented shows that a combination of kinetic measurements and model dynamic calculations reveals many of the unique characteristics of low-temperature chain solid-state reactions. The local lattice deformations, resulting in a closely packed complex, along with high amplitudes of intermolecular reactant vibrations, provide a high value of the rate constant in the low-temperature plateau region, which is several orders of magnitude greater than in some of intra- and intermolecular hydrogen atom transfer reactions (see refs.2,3). The proposed algorithm for calculating the tunneling transition probability can be used in descriptions of other reactions, including specific low-temperature critical phenomena.

The use of the matrix isolation technique to separate the chain initiation and chain growth stages, and to prepare perfectly ordered structures has allowed us to enlarge the number of objects and to investigate new reactive condensed systems with regular crystalline or fractal structures.

The authors are grateful to Academician V.I. Goldanskii, Dr. D.E.Makarov, and Prof. S. Sato for useful discussion and to A.U.Goldschleger for assistance with the experiments.

References

1. V. I. Goldanskii, *Dokl. Akad. Nauk SSSR* 1959, **124**, 1261; **127**, 1037 [*Dokl.Chem.* (Engl. Transl)].
2. V. I. Goldanskii, V. A. Benderskii, and L. I. Trakhtenberg, *Adv. Chem. Phys.*,1989, **75**, 349.
3. V. I. Goldanskii and V. A. Benderskii, *Int.Rev.Phys.Chem.*, 1992, **11**, 1.
4. V. A. Benderskii,V. I. Goldanskii, and A. A. Ovchinnikov, *Chem. Phys. Lett.*, 1980, **73**, 492.
5. V. A. Benderskii, D. E. Makarov, and P. G. Grinevitch, *Chem.Phys.*, 1992, (in press).
6. V. A. Benderskii, E. Ya. Misochko, V. A. Titov, P. G. Filipov, and V. A. Filipov, *Izv. Akad. Nauk. Ser.Khim.* 1992, 2268 [*Bull. Acad. Sci. Div. Chem. Sci.*].
7. V. A. Benderskii, P. G. Filipov, E. Ya. Misochko, A. A. Ovchinnikov, *Pis'ma v ZhETF*, 1980, **32**, 429.
8. I. M. Barkalov, V. I. Goldanskii, D. P. Kirykhin, and A. M. Zanin, *Int. Rev.Phys. Chem.*, 1983, **3**, 247.
9. V. A. Benderskii, A. A. Ovchinnikov, and P. G. Philippov, *Reactivity of Solids*, 1988, **4**, 228.
10. T. J. Tauge and C. A. Wight, *Chem. Phys.*, 1991, **156**, 288.
11. T. G. Tauge, P. M. Kligmann, C. P. Collier, M. A. Ovchinnikov, and C. A. Wight, *J. Phys. Chem.*, 1992, **96**, 1288.
12. V. A. Benderskii, E. Ya. Misochko, P. G. Filipov, and *Khim. Fizika,* 1986, **5**, 995 [*Chemical Physics* (Engl. Transl)].
13. A. J. Sedlacek and C. A. Wight, *J. Chem. Phys.*, 1988, **88**, 7418.
14. C. A. Wight, P. M. Kligmann, T. R. Botcher, and A. J. Sedlacek, *J. Phys. Chem.*, 1990, **93**, 2487.
15. N. N. Semenov, *Chemistry and Technology of Polymers*, 1960, **7—8**, 196.
16. O. Hassel and C. Romming, *Quart. Rev.*, 1962, **14**, 1.
17. V. A. Benderskii, V. I. Goldanskii, D. E. Makarov, and E. Ya. Misochko, *Chem. Phys. Lett.*, 1991, **179**, 334.
18. Ya. M. Kimmelfeld, E. V. Lumer, and A. P. Shwedchikov, *Chem. Phys. Lett.*, 1973, **21**, 429.
19. G. B. Sergeev, Ya. M. Kimmel'fel'd, and M. I. Shilina, *Khim. Fizika*,1983, **2**, 703 [*Chemical Physics* (Engl. Transl)].
20. V. A. Titov, P. G,Filipov, E. Ya. Misochko, R. D. Usmanov, and V. A. Benderskii, *Dokl. Akad. Nauk SSSR*, 1986, **290**, 1414 [*Dokl.Chem.* (Engl. Transl)].
21. R. Eckling, *Chem. Ber.*, 1960, **B93**, 3014.
22. G. M. Wieder and D. A. Dows, *J. Chem. Phys.*, 1962, **37**, 2990.
23. R. Honig and H. Hook, *RCA Rev.*, 1960, 360.
24. M. E. Fajardo, R. Nhithall, J. Feld, F. Okada, and V. A. Abrakian, *Laser Chem.*, 1988, **9**, 1.
25. H. Kunz and J. G. McCaffrey, *J. Chem. Phys.*, 1991, **94**,1039.
26. V. G. Dashevskii, *Zh. Strukt. Khim.* 1970, **11**, 913 [*J. Struct. Chem.* (Engl. Transl)].
27. N. F. Stepanov, O. E. Gishina, G. B. Sergeev, and V. V. Smirnov, *Adv. Mol. Relax. Int. Proc.*, 1978, **12**, 325.
28. B. Nelander, *Theor. Chim. Acta,* 1972, **25**, 382.
29. J. Prisette, G. Seger, and E. Kochansky, *J. Am. Chem. Soc.,* 1978, **110**, 6941.
30. G. Wegner, *Macromolec. Chem.,* 1971, **145**, 85.
31. H. Eyring and M. Z. Polanyi, *J. Phys. Chem.*, 1931, **B12**, 279.
32. S. J. Sato, *J. Chem. Phys.*, 1955, **23**, 592, 2456.
33. W. N. Lipscomb and F. E. Wang, *Acta Cryst.*, 1961, **14**, 1100.
34. V. A. Benderskii, V. I. Goldanskii, and D. E. Makarov, *Chem. Phys.*, 1992, **159**, 29.
35. M. Ya. Ovchinnikova, *Chem. Phys.*, 1979, **36**, 85.
36. W. H. Miller, *J. Chem. Phys.*, 1975, **63**, 1166.
37. V. K. Babamov and R. A. Marcus, *J. Chem. Phys.*, 1981, **74**, 1790.
38. W. H. Miller, *J. Phys. Chem.*, 1983, **87**, 3811.
39. S. Levit, J. W. Negele, and Z. Pattiel, *Phys. Rev.*, 1980, **C22**, 1979.

Received July 21, 1992.